Materials Advances

ROYAL SOCIETY OF CHEMISTRY

PAPER

View Article Online
View Journal | View Issue

Check for updates

Cite this: *Mater. Adv.*, 2022, 3, 2918

Supercritical CO_2 blown poly(ε-caprolactone) covalent adaptable networks towards unprecedented low density shape memory foams†

Maxime Houbben, Jean-Michel Thomassin and Christine Jérôme *

Received 13th January 2022,
Accepted 20th February 2022

DOI: 10.1039/d2ma00040g

rsc.li/materials-advances

Recent studies have highlighted the efficacy and benefit of shape-memory polymer foams over bulk materials, especially for self-deploying medical devices. In that field, poly(ε-caprolactone) covalent adaptable networks (PCL-CAN) are materials of choice since they combine biocompatibility, excellent shape memory properties with reconfiguration ability of the network allowing the design of biomedical devices of complex shapes. The preparation of PCL-CAN foams was here investigated by using a solvent-free supercritical CO_2 foaming process. Starting from a mixture of low molar mass PCL stars bearing furan or maleimide as end-groups, a two-step foaming process was developed that leads to highly porous foams of unprecedented low density (0.02 g cm^{-3}). We took advantage of the thermoreversible Diels–Alder addition to control the molar mass and the network crosslinking density of the PCL throughout the foaming process. Adjusting the amount of Diels–Alder adducts at each foaming step is key to allow foaming of the mixture and reach closed-cell foams of low density that exhibit excellent shape memory properties. Thanks to the thermoreversibility of the Diels–Alder reaction, these foams are also recyclable at high temperature. These innovative shape memory PCL-CAN foams are attractive candidates as self-deploying implants for vessels occlusion, as shown by dynamic mechanical analysis and illustrated by mechanical occlusion of a large simulated vessel.

Open Access Article. Published on 22 February 2022. Downloaded on 9/6/2025 6:56:05 AM.
This article is licensed under a Creative Commons Attribution-NonCommercial 3.0 Unported Licence.

Introduction

Polymer foams are versatile materials that allow combining the advantageous properties offered by polymers with the remarkable properties of their intrinsic architecture giving attractive lightweight materials with high mechanical strength.[1] In the past years, the design of porous materials by environmental friendly foaming processes provided foams of many thermoplastics covering a wide range of applications in various fields, from materials science to medicine.[1–7] In the latter, biodegradable foams are particularly interesting to design implants for therapeutic purposes[8–10] as well as scaffolds for tissue engineering.[11–13] Among the biodegradable materials used for biomedical purposes, semi-crystalline poly(ε-caprolactone) (PCL) has been widely studied because of its biocompatibility and remarkable mechanical properties afforded by a low glass transition temperature ($T_g \sim -60$ °C) and a melting temperature easily achieved above the body temperature ($T_m \sim 60$ °C). Furthermore, when PCL is chemically crosslinked, the resulting covalent networks exhibit excellent shape memory properties, making them particularly appealing for the development of the mini-invasive surgery making available self-deploying devices.[14] For example, easy-to-implement endovascular occlusion systems rely on the delivery of a temporary low-volume SMP foam to the confined space of a vessel where, when in place, an externally triggered expansion shifts the foam to its original expanded shape, so filling the vessel.[15]

Therefore, many processes have been studied and developed to get porous structures of PCL. Among the diverse foaming processes, the solvent-free supercritical CO_2 ($scCO_2$) foaming received great emphasis;[3,16–24] CO_2 being non-toxic, non-flammable, and inexpensive.[23–26] As illustrated in Table 1 that gathers some reported foaming conditions and the corresponding PCL foams characteristics, this $scCO_2$ process leads to PCL foams of low density (lower limit about 0.2 g cm^{-3} which corresponds to 80% porosity) in mild conditions, namely by processing the PCL at a temperature between 30 to 65 °C in a pressure range from 10 to 20 MPa with variable depressurization rates.[27–34] Table 1 also evidences that PCL with a molar mass above 40 kg mol^{-1} is required in order to get enough chain entanglement to insure an appropriate viscosity to sustain the expansion during the depressurization. On the other hand, if the viscosity would be too high, it would limit the material expansion preventing to achieve low density foams. Therefore, the preparation

Center for Education and Research on Macromolecules (CERM), University of Liege (ULiege), CESAM-RU, Sart-Tilman, Building B6a, B-4000 Liege, Belgium. E-mail: c.jerome@uliege.be

† Electronic supplementary information (ESI) available. See DOI: 10.1039/d2ma00040g

© 2022 The Author(s). Published by the Royal Society of Chemistry

Open Access Article. Published on 22 February 2022. Downloaded on 9/6/2025 6:56:05 AM.
This article is licensed under a Creative Commons Attribution-NonCommercial 3.0 Unported Licence.

Table 1 Summary of some reported PCL foams of low density obtained *via* a supercritical CO_2 process

Material and additives	M_w (kDa)	Density (g cm^{-3})	Porosity (%)	$ScCO_2$ pressure (MPa)	Foaming T^0 (°C)	Depressurization rate (MPa s^{-1})	Ref.
PCL	50	0.29–0.35	68–72.5	14	39	5	19
PCL	45	0.07–0.72	36.7–93.8	10–15	31.5–65	5	27
PCL	45	0.2–0.5	55–85	20	50	0.02	28
PCL	80	0.22	80	5–20	40–50	7–12	29
PCL/DXMT/glycofurol	48–90	0.29–0.93	18.5–74.5	20	45	0.016–0.05	30
PCL/PEO	50–70	0.103	80–94.6	10–17	45–95	Fast	31
PCL/HA nanocomposites	65	0.2–0.5	55–85	10–20	37–40	0.02–10	32
PCL/ethanol	80	0.22–0.42	62–80	12.3–20.5	35–45	0.24–4.1	33
PCL/MWNT	50	0.18–0.31	72–84	20	60	10	34

of crosslinked PCL foams by this process is scarcely described[25] and relies mostly on post-foaming crosslinking treatment. Until now, foaming processes rather include microwave assisted solvent foaming, high internal phase emulsion, particle leaching or glass microsphere incorporation when the preparation of porous PCL covalent networks is foreseen.[33,35–39]

Introducing adaptable crosslinks in polymer materials allows today to resolve the intersection between thermoplastics and thermosets.[40,41] Advantageously, shape-memory polymers based on covalent adaptable networks (CAN) have emerged since they remarkably combine efficient shape memory properties with reconfiguration and/or recycling capabilities.[42] Indeed, these CANs make possible the reprocessing of the permanent shape so as the full recycling of cross-linked scrapes (*e.g.* resulting of processing). They are thus eco-friendlier than the non-reversible covalent networks. In addition, they are preferred when shape memory devices of complex design are foreseen for their reconfiguration ability which facilitates their manufacturing.[43] In that frame, some of us[44–46] have reported the synthesis of PCL-CANs with remarkable shape memory properties by melt blending 4-arm PCL stars bearing either furan or maleimide moieties at their chain-ends, which leads to the formation of thermo-reversible network.

In this paper, we are taking advantage of the temperature-controlled equilibrium of the Diels–Alder cycloaddition to tune the content of Diels–Alder adducts in the furane/maleimide PCL stars mixture. As a consequence, the mixture viscosity and the material crosslinking degree can be adjusted in function of the $scCO_2$ foaming step requirements. In a first step, the partial formation of Diels–Alder adducts allows the coupling of the PCL stars increasing their molar mass and so the viscosity of the material. This allows $scCO_2$ blowing and the formation of PCL foams stabilized by the PCL crystallization occurring upon venting.[47–49] Then, the stabilization of the expanded foams is improved by increasing further the Diels–Alder adducts content until maximum crosslinking of the foamed PCL is reached. This crosslinking ensures the foams stability above T_m providing them shape memory properties and leading to potential biomedical application as self-deploying implant for vessels occlusion.

Experimental section

Materials

All the PCL stars used in this work were obtained by end-groups functionalization of commercially available star-shaped PCL samples (CAPA™ 4801, kindly offered by Perstorp® UK limited) according to a previously reported procedure.[47] All the characteristics of the used PCL stars are reported in the Table 2. PCL 80 000 g mol^{-1} (PCL_{700}-2OH – Aldrich), CO_2 (Air Liquide), 4, 4′-methylenebis(cyclohexyl isocyanate) (Acros Organics) and chloroform (VWR) were used as received.

Preparation of PCL disks

PCL-CAN disks: stoichiometric amounts in reactive groups (furan and maleimide moieties) of PCL_{76}-4FUR and PCL_{76}-4MAL (Table 2) powders were grinded together in a mortar in order to get 4 g of mixture. This mixture was melt-blended at 125 °C in a 6 cm^3 co-rotating twin screw mini-extruder (Xplore, DSM) for 10 min at 150 rpm. After extrusion, the polymer blend was let to cool down to room temperature. Then, the blends were displayed into a disk mold (8 mm in diameter and 0.5 mm in thickness), heated at 105 °C and compressed under a load of 75 N for 90 seconds. They were then quickly cooled down to room temperature, extracted from the mold and stored at −20 °C under a dry atmosphere. Just before foaming, a 60 min. Thermal treatment at 105 °C was applied to these disks placed back in the mold in order to adjust the cross-linking degree of these PCL-CANs. The optimal time of 60 min was experimentally determined.

PCL-PU disks: PCL_{76}-4OH was melted in a beaker at 60 °C under stirring and then 4,4′-methylenebis(cyclohexyl isocyanate) (0.6 equivalent) was added. After 30 seconds of stirring, the mixture was poured into a flat sheet mold (50 × 50 mm with a thickness of 0.5 mm) and compressed under a load of 75 N for 90 seconds. Disks (8 mm in diameter and 0.5 mm in thickness) were then cut from this sheet.

Table 2 Macromolecular parameters of the starting PCL stars

Code	End-group function	M_n[a] (g mol^{-1})	Funct.[b] (%)	Cryst.[c] (%)	Melting point (°C)
PCL_{76}-4OH	Hydroxyl	8800	100	55	49.59
PCL_{76}-4FUR	Furan	9500	95	43	46.91
PCL_{76}-4MAL	Maleimide	9600	81	39	45.30

[a] As determined from ^{1}H NMR including chain-ends. [b] Degree of functionalization of the PCL chain-ends measured by ^{1}H NMR. [c] Crystallization degree as determined from DSC analysis.

Open Access Article. Published on 22 February 2022. Downloaded on 9/6/2025 6:56:05 AM.
This article is licensed under a Creative Commons Attribution-NonCommercial 3.0 Unported Licence.

PCL_{700}-2OH ($M_n \sim 80.000$ g mol^{-1}) disks: they were prepared by direct hot molding of the material into a disk mold (8 mm in diameter and 0.5 mm in thickness).

Supercritical CO_2 foaming process

The PCL disks were introduced in a 316 stainless steel high pressure reactor (100 mL) from Parr Instruments, for $scCO_2$ foaming. First, the reactor was thermostatically controlled at 65 °C in an oil bath for 30 min. Then, a CO_2 pressure of 25 MPa was applied with an ISCO 260D high pressure syringe pump for 15 min. This step was followed by a rapid decompression in a few seconds to ambient pressure. Finally, the reactor was let in an oil bath at 40 °C for 5 minutes. The final foams were then collected from the reactor. These foaming pressure and temperature were optimized in this study.

Foams characterization

Foams density (ρ_F) was determined as the ratio between the mass and volume of the sample. The mass was measured by using a high accuracy balance and the volume is measured by pycnometry using water as liquid of known density at 25 °C. Each foam was weighted prior and after analysis to confirm that the closed cell porosity and water being non-wetting for PCL were enough to ensure no penetration of the liquid inside the foam. The porosity of the foams, expressed in %, was then calculated by the following eqn (1):

$$\text{Porosity} = \left(1 - \frac{\rho_F}{\rho_P}\right) \times 100 \quad (1)$$

where ρ_F is the density of the foam, ρ_P is the density of the bulk PCL (*i.e.* 1.14). The expansion ratio of the foams was calculated according to eqn (2).

$$\text{Expansion ratio} = \frac{\text{Initial disk density}}{\text{Foamed disk density}} \quad (2)$$

Scanning electron microscopy (SEM) was used to determine the cells size and morphology of the produced foams using an acceleration voltage of 20 keV. The samples were mounted on metal holder and fixed using a double-sided adhesive tape. Samples cross-section were vacuum-coated with a layer of gold prior to analysis with a FEI-Phillips Quanta 600 microscope using an acceleration voltage of 20 kV.

PCL network characterization

Swelling experiments were performed to evaluate the cross-linking density of the PCL networks. The samples were weighted (initial material weight) and then placed in $CHCl_3$ for 24 h at room temperature. The swollen samples (gels) were weighted (swollen network weight). These gels were then dried under vacuum for 24 h and weighted (dried network weight). From these data, the swelling ratio and the insoluble fraction of the networks were calculated based on the eqn (3) and (4).

$$\text{Swelling ratio}(\%) = \frac{(\text{swollen network weight} - \text{dried network weight})}{\text{dried network weight}} \times 100 \quad (3)$$

$$\text{Insoluble fraction}\ (\%) = \frac{\text{dried network weight}}{\text{initial material weight}} \times 100 \quad (4)$$

The conversion of the furan end-groups into Diels–Alder adducts within the cross-linked materials was evaluated by Raman spectroscopy as already described elsewhere.[47] Raman spectra were recorded at room temperature using a Horiba-Jobin-Yvon Labram 300 confocal spectrometer equipped with an Olympus BX40 microscope. A Spectra Physics model 168 Krypton ion laser with a 647.1 nm line was focused on the different samples with an Olympus_50 objective. The laser power at the sample level was of the order of 15 mW. The spectrum was accumulated twice for 20 s. The detector is an Andor iDus BRDD 401 CCD. All spectra baselines were corrected using a home-made software. After normalization of the spectra on the PCL band at 1750 cm^{-1}, the furan conversion is estimated by measuring the intensity of the band at 1503 cm^{-1} (I) typical for the furan ring and for the starting PCL_{76}-4FUR by applying eqn (5). Measurements of the number average molar mass (M_n) and polydispersity were carried out by size exclusion chromatography (SEC) in THF (flow rate: 1 mL min^{-1}) at 45 °C using a viscotek 305 TD liquid chromatograph equipped with two PSS SDV linear M columns calibrated with poly(styrene) standards.

$$\text{Conversion}\ (\%) = \frac{I \text{ on PCL stars mixture spectrum}}{\frac{I}{2} \text{ on } PCL_{76}\text{-4FUR spectrum}} \times 100 \quad (5)$$

Shape memory characterization

The shape memory properties, namely, the fixity of the temporary shape (*i.e.* the capacity of the foam to retain the temporary shape when the stress is released below T_m) and the recovery of the permanent shape (*i.e.* the fidelity of the recovered permanent shape after 1 SM cycle) of the PCL-CAN foams were determined by thermo-mechanical traction analysis using a TA Q800 DMA equipment. The foam sample was cut (1 × 0.5 × 0.5 cm cutted foam), clamped and equilibrated at 65 °C in the DMA. Then, it was sequentially elongated up to 0.03 MPa following a controlled stress ramp (0.03 MPa min^{-1}), then cooled down to 0 °C at 3 °C min^{-1} before releasing the stress. The comparison of the strain at 0 °C before and after the release of the stress allows measuring the sample fixity. The fixity ratio (R_f) is given by eqn (6). Finally, the sample is heated again to 65 °C at 3 °C min^{-1} in order to allow the sample to recover its permanent shape. The shape recovery is obtained by comparing the strain at 65 °C before and after this cycle, the recovery ratio (R_c) being calculated by eqn (7). This shape memory cycle was repeated 4 times.

$$R_f = \frac{\text{strain after stress release at 0 °C}}{\text{strain before stress release at 0 °C}} \times 100 \quad (6)$$

© 2022 The Author(s). Published by the Royal Society of Chemistry

Open Access Article. Published on 22 February 2022. Downloaded on 9/6/2025 6:56:05 AM.
This article is licensed under a Creative Commons Attribution-NonCommercial 3.0 Unported Licence.

$$R_c = \frac{\text{strain at } 65\ ^{C} \text{ without stress for cycle } N \text{ at } 0\ ^{C}}{\text{strain at } 65\ ^{C} \text{ without stress for cycle } (N-1)} \times 100 \quad (7)$$

Results and discussion

Foaming of PCL-CAN

As previously reported,[45] PCL-CAN can be prepared by melt blending a mixture of 4-arm PCL stars bearing maleimide or furan moieties at the chain-ends in a stoichiometric amount. By controlling the temperature, a thermo-reversible PCL-CAN is obtained by the formation of Diels–Alder adducts below 125 °C between both types of stars (Fig. 1, insert). This network can be cleaved back to a fluid mixture of the stars by heating above 125 °C. With the goal to get foams of this material, a stoichiometric mixture of 4-arm PCL stars (~9 kDa) bearing maleimide or furan moieties at their chain-ends was hot-melt blended, then hot molded as a disk and kept 1 h at 105 °C before $scCO_2$ foaming (Fig. 2a). Based on literature data (Table 1), these disks are placed under 25 MPa of CO_2 at 65 °C (*i.e.* above the melting temperature) in order to dissolve $scCO_2$ into the molten material. Then, CO_2 gas expansion is induced by the rapid depressurization of the vessel, leading to the disk foaming. When these disks are thermostatized 30 min. At 65 °C in the high pressure reactor before pressurization, a foam exhibiting an unprecedented low density is remarkably obtained (Fig. 2b). If the same process is performed with PCL stars exhibiting OH groups at the chain-ends and therefore unable to react together, no foaming is observed at the end of the process. This is expected for low molar mass materials due to the limited chain entanglement leading to too low melt strength to get stable foam. When this process is applied to a disk of linear PCL of high molar mass (80 kDa), a foam is obtained (Fig. 2e) but exhibiting a much lower expansion as compared to the PCL-CAN. Indeed, a density of 0.16 g cm^{-3} is measured for the linear PCL foam which is in line with reported literature data, while remarkably, the volume expansion is very high for the PCL-CAN, leading to foams with a very low density of 0.02 g cm^{-3} (Table 3). This behavior originates from the peculiar feature of the thermo-reversible Diels–Alder (DA) reaction which allows tuning of the molar mass and network

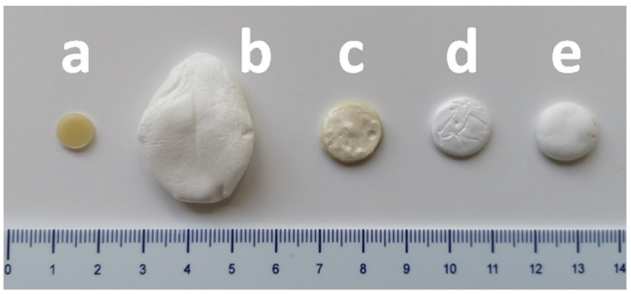

Fig. 2 (a) PCL-CAN disk before foaming, and foams of (b) PCL-CAN disk cured at 105 °C for 1 hour, (c) PCL-CAN disk cured at 65 °C for 72 hours, (d) PCL-PU network, (e) linear high molar mass PCL.

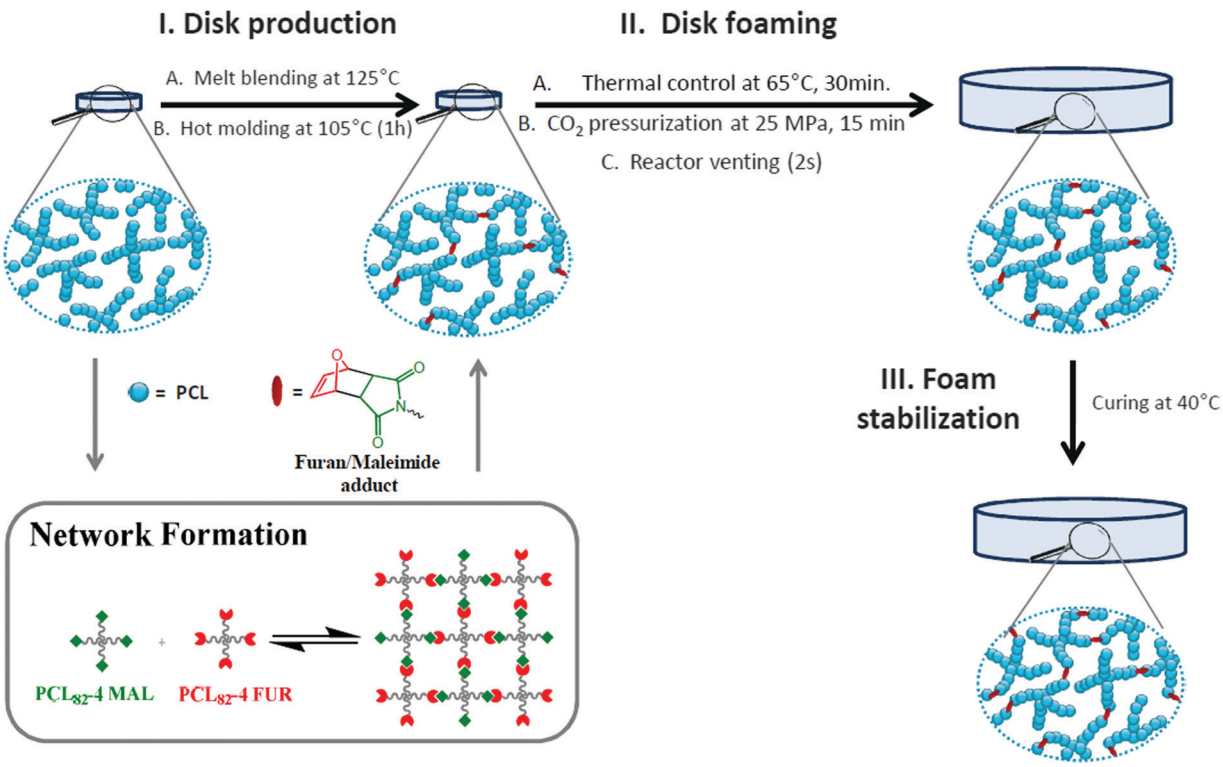

Fig. 1 Sketch of the progressive network formation in function of the different steps of the PCL-CAN foaming and crosslinking starting from the PCL-CAN precursors.

Open Access Article. Published on 22 February 2022. Downloaded on 9/6/2025 6:56:05 AM.
This article is licensed under a Creative Commons Attribution-NonCommercial 3.0 Unported Licence.

Table 3 Foams density and expansion ratio of various PCL disks

Disk used for foaming	Density (g cm^{-3})	Porosity (%)	Expansion ratio
1. PCL-CAN disk before foaming	1.14	—	—
2. PCL-CAN cured at 105 °C for 1 h.	0.02	98.2	58
3. PCL CAN cured at 65 °C for 72 hours	0.23	80	5
4. PCL-PU network	0.23	80	5
5. Linear PCL 80.000 g mol^{-1}	0.16	86	7

crosslinking density of the stars mixture by adjusting the thermal treatment of the disk. As sketched in Fig. 1, the starting stars mixture is initially not foamable due to the low melt strength of the short-arm stars. By taking advantage of the DA reaction, the matrix strength can be increased by formation of Diels–Alder adducts between stars, increasing the molar mass. Therefore, the disks are first hot molded at 105 °C for 60 minutes before placing them, at 65 °C for 30 min in the high pressure reactor before pressurizing with $scCO_2$. To follow this thermal process is crucial since it forms an optimal number of DA adducts so that the resulting molar mass is on one side increased enough to insure a melt strength allowing foaming but on the other side is kept low enough to reach high foam expansion. Indeed, as evidenced on Fig. 2c, when a disk is cured for a much longer time, *e.g.* 72 h, at 65 °C instead of 30 min, the material expansion remains limited during foaming. This is explained by the crosslinking of the material reached before foaming thanks to the long curing time at 65 °C. This is supported by the similar expansion observed for a PCL-PU network crosslinked by diisocyanate before foaming (Fig. 2d). Table 3 summarizes the foams densities and expansion ratios of these samples and evidences the critical role of crosslinking on the foam expansion. When the material is highly crosslinked before foaming, whatever the used chemistry (reversible *vs.* irreversible bonds), the foam expansion is limited.

Fig. 3 shows the expansion ratio of PCL-CAN foams obtained for disks hot molded for various time at 105 °C. It clearly evidences the impact of the thermal treatment of the disks on their foaming capacity, the maximum expansion being

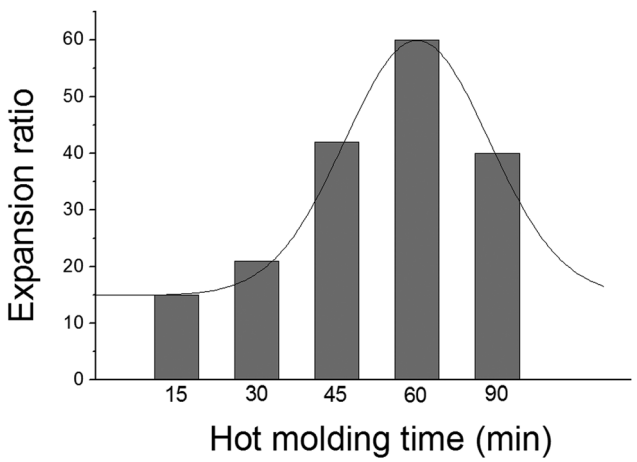

Fig. 3 Expansion ratio of PCL foamed at 65 °C in function of hot molding time at 105 °C.

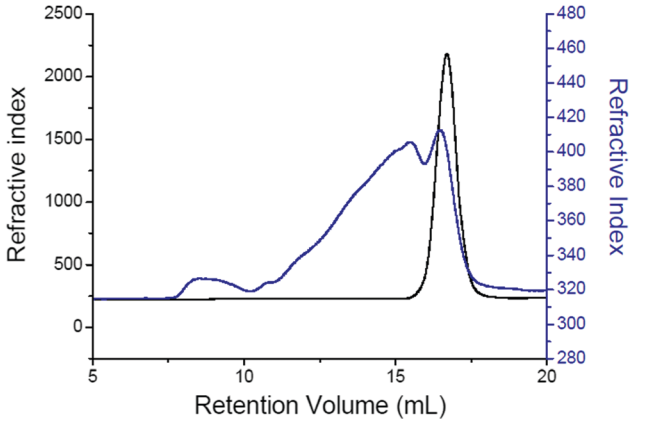

Fig. 4 SEC chromatograms of a PCL stars mixture before hot molding (before step I, Fig. 1) (black) and after hot molding, reactor thermostatization, pressurization and venting (after step II, Fig. 1) (blue).

observed for a curing time of 60 minutes. The increase of the molar mass without reaching crosslinking of the sample has been evidenced by swelling tests, SEC and Raman spectroscopy.

After hot molding for 1 h at 105 °C, the disk remains fully soluble in chloroform. At that temperature a few Diels–Alder adducts are formed leading to chain extension but a network is not achieved. After thermostatization for 30 min in the high pressure cell at 65 °C and impregnation for 15 min in $scCO_2$, the material does not dissolve anymore but highly swells in $CHCl_3$ forming a very fragile jelly fish structure difficult to handle, characteristic of a network of very low crosslinking density. This sample was also analyzed by size exclusion chromatography (SEC) after dispersion/swelling in THF. The SEC analysis of the soluble fraction remaining after filtration on a 2 micron filter (*i.e.* 26.9 wt%) confirms the increase of the molar mass of the sample by the broad trace at low elution volume (Fig. 4). It also reveals that some unreacted stars are still present in the sample.

In previous work, Raman Spectroscopy demonstrated to be a powerful tool to follow the formation of the DA adduct in this PCL matrix.[46] Typically, the three functional groups of interests (furan, maleimide and DA adduct) can be distinguished in the Raman spectrum and the conversions of the furan and maleimide end-groups into corresponding DA adducts can be quantitatively measured. Raman analyses were performed at each step of the process and the results can be seen on Table 4.

Table 4 Raman study of the PCL-CAN foaming process

Foaming step	Treatment		Furan conv. (%)
1.	Disk production	1 h, 105 °C	16
2.	Disk foaming	30 min, 65 °C 15 min, 65 °C, 25 MPa of $scCO_2$ Venting	24
3.	Foam stabilization	40 °C, 7 days	62
	Disk not foamed	40 °C, 7 days	63

© 2022 The Author(s). Published by the Royal Society of Chemistry

Open Access Article. Published on 22 February 2022. Downloaded on 9/6/2025 6:56:05 AM.
This article is licensed under a Creative Commons Attribution-NonCommercial 3.0 Unported Licence.

After hot molding, the conversion of both maleimide and furan moieties into DA adducts is 16% (Fig. 1 – disk production). It points out that after processing, a few DA adducts are formed, which is in line with the full solubility of the processed disk. After thermostatization in the $scCO_2$ reactor at 65 °C, and impregnation in supercritical CO_2 for 15 min, the DA adduct conversion increases to 24% (Fig. 1 – disk foaming) but remains below the gel point of this PCL_{76}-4MAL and PCL_{76}-4FUR mix that is about 33% of DA conversion.[46] This confirms that foaming occurs when the molar mass of the sample is higher than the one of the starting stars, but before the formation of the network which accounts for the exceptionally high volume expansion. Let us mention that both the synthesized PCL-PU as well as the PCL-CAN let 72 h at 65 °C exhibit the same swelling ratio of 1500% in $CHCl_3$ and an insoluble fraction of 97%. This demonstrates that a network was formed through the whole disks before foaming, which explains the limited foam expansion observed in these cases.

Finally, after $scCO_2$ foaming, an additional curing step is performed at 40 °C with the purpose to increase the DA adducts conversion and reach the network formation to stabilize the foamed structure (Fig. 1 – foam stabilization). After 7 days of curing at 40 °C, the DA adducts conversion levels up at 62% which is in good agreement with the values reported under the same conditions by previous works.[46] Interestingly, a similar conversion is achieved for a non-foamed PCL-CAN disk experiencing the same thermal curing which confirms that foaming does not alter the Diels–Alder reaction.

At the term of the foaming process, the morphology of the scaffolds was observed by scanning electron microscopy (SEM). Fig. 5 shows the SEM micrographs of the cross-section of the foam revealing a porous closed cell morphology with pores of a hundred of microns. This is in line with reported $scCO_2$ foaming with low soaking time and high depressurization rate[50] and follows the predictions of the nucleation theory.[51,52] If a few pores allow some interconnexions between adjacent cells, most of them are closed as usually observed for the $scCO_2$ foaming process. Thanks to this closed-cell structure, good mechanical properties are preserved for these extremely expanded foams. We observe a young modulus of 0.04 MPa in compression at r.t. allowing the maintain structural integrity to withstand blood pressure.

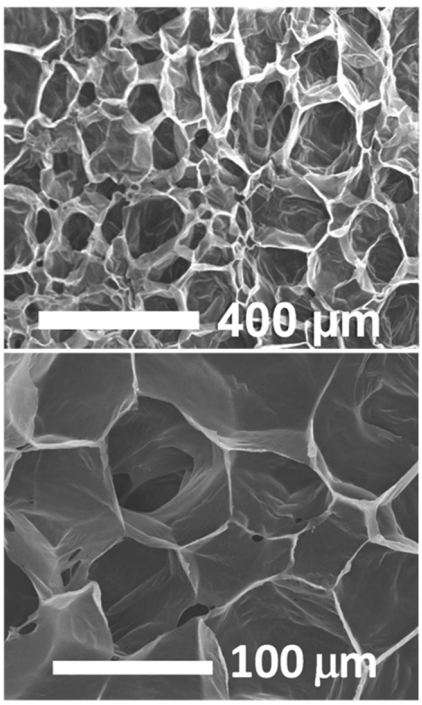

Fig. 5 SEM analysis of foamed PCL-CAN after a hot molding of 1 hour at 105 °C and foaming at 65 °C.

Foam thermal stability and reprocessing

The advantage of getting a covalent PCL network after the material foaming is that crosslinking preserves the foam structure above the melting temperature. This thermal stability was demonstrated by placing foamed samples at 80 °C for 15 minutes and determining the volume expansion retention (VER) after thermal treatment according to eqn (8).

$$\mathrm{VER} = \frac{\text{Expansion ratio after thermal treatment}}{\text{Initial expansion ratio}} \times 100 \quad (8)$$

Fig. 6a shows the effect of the foam curing time at 40 °C on the VER. Without a curing period at 40 °C after foaming, the foam structure is lost as soon as the PCL is molten traducing

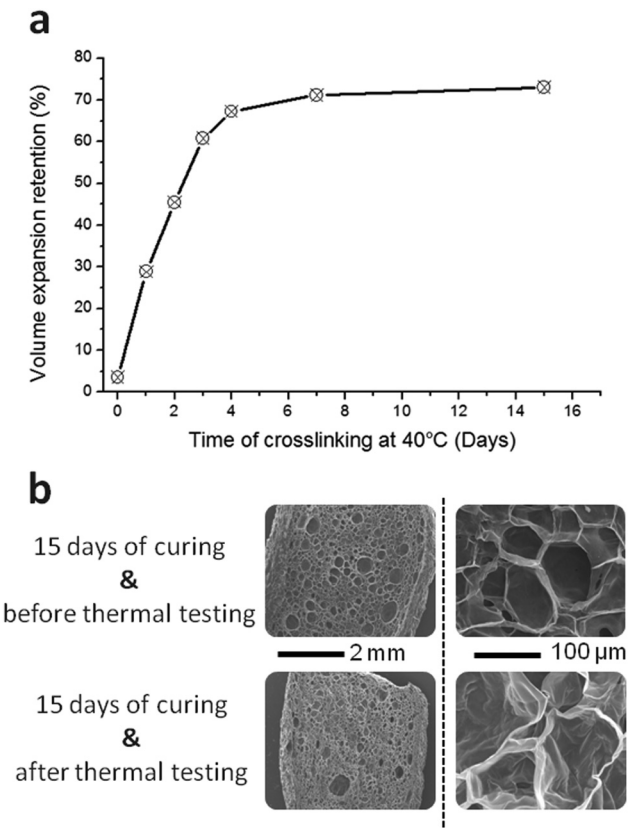

Fig. 6 PCL-CAN foam thermal stability assessment: (a) VER in function of the curing time at 40 °C after foaming and (b) SEM micrographs of the cross-section of a foam cured for 14 days, before (top) and after (bottom) heating at 80 °C for 15 min.

Open Access Article. Published on 22 February 2022. Downloaded on 9/6/2025 6:56:05 AM.
This article is licensed under a Creative Commons Attribution-NonCommercial 3.0 Unported Licence.

the absence of crosslinking as evidenced in the previous section. A curing time above 4 days allows to reach a maximum crosslinking of the material which is then able to retain more than 70% of its expansion. SEM micrographs of the cross-section of the foam before and after thermal testing (Fig. 6b) on a sample cured for 14 days show that the foam structure is well preserved for the crosslinked PCL-CAN.

The decrease of the foam expansion at 80 °C is caused by the disappearance of the PCL crystalline regions leading to the softening and relaxation of the cell walls. The network relaxation has previously been described by the loss of oriented crystallization occurring when the material crystallizes under load. This is the case when the crystallization occurs during the expansion of the material under foaming.[53,54] Thus, when such foam is placed over T_m, the load that was induced by foaming being no longer present, chain relaxation can occurs. Once the sample goes back under T_m, crystallization is no more oriented leading to a partial decrease of the foam porosity. Nevertheless, thanks to the induced crosslinking at the foamed state, the foam architecture is maintained. The stabilizing effect of the network formation is well represented on Fig. 6 where low curing times lead to low volume expansion retention. The volume reduction is less and less significant upon curing resulting in about 70% of the initially expanded volume after 7 days. Even with this expansion reduction, the density is still low reaching 0.03 g cm^{-3}.

Besides, an additional advantage of these PCL-CAN is the reversible thermal cleavage of the DA adducts at high temperature allowing full reprocessing of the material.[44] The reprocessability/recyclability of the foamed PCL-CAN was confirmed by heating the sample at 125 °C for 1 hour. A fluid mixture is then obtained that can be reprocessed as a foam by following the developed protocol. The expansion ratio of the recycled material reached 54 that is very close to the one to the pristine material (*i.e.* 58). A VER of 73 is obtained for foams of the recycled material and cured at 40 °C for 14 days that is also comparable to the value of 76 obtained from a pristine stars mixture. This is another evidence that the foaming process based on $scCO_2$ is not altering the Diels Alder reaction so that the PCL-CAN fully preserves its network adaptability and reprocessability.

Shape memory properties of PCL-CAN foams

Fig. 7 shows 4 consecutive shape memory cycles of the PCL-CAN foam crosslinked during 7 days. Upon cooling under constant stress, the sample experiences a large increase of its deformation between 35 °C and 15 °C resulting from the growth of crystallites oriented along the stretching direction. This observation is similar to the behavior of non-foamed PCL-CAN samples.[53,54] A very high fixity (above 99%, Table 5) is obtained for each cycle thanks to the foam crystallinity, which is also in line with non-foamed PCL films.

The foams shape recovery is trigger by a temperature above 45 °C. As shown in Table 5, the first cycle is characterized by a lower shape recovery (91%), known as training phenomenon,[55] while the following cycles are characterized by excellent recovery ratios close to 97%, which is very close to the already demonstrated properties of PCL-CAN films.[46] It can be observed on Fig. 7 that, the deformation obtained at 65 °C increases with the number of cycles. This particular phenomenon also observed for PCL-CAN film[46] can attributed to the occurrence of some retro-DA reactions triggered at 65 °C under stress. In addition, some gas leaching can occurs from the foam because of the network relaxation caused by the rupture of some DA adducts. The material becomes more ductile and stretches then more. Nevertheless, this phenomenon is attenuated with the number of cycles and do not affect the shape recovery.

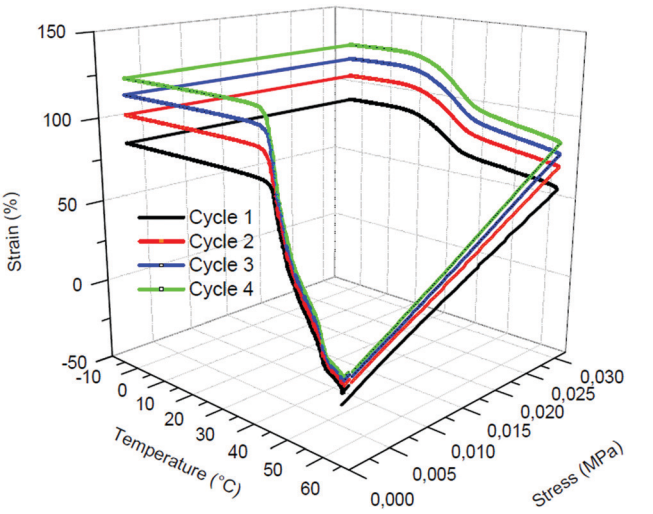

Fig. 7 Shape-memory properties evaluated by thermo-mechanical cycling of PCL-CAN foam after 7 days of curing.

Table 5 Shape memory properties of PCL-CAN foam

Cycle	1	2	3	4
Fixity ratio, R_f (%)	99.4	99.5	99.5	99.5
Recovery ratio, R_c (%)	91.18	96.78	97.5	98.18

Thanks to their demonstrated shape memory properties, the PCL-CAN foams developed in this study can be very attractive for various biomedical applications. As an example, the potential of these foams for vessel occlusion applications[56] was qualitatively demonstrated (Fig. 8). For that purpose, a cylindrical monolith of PCL-CAN foam was cut with a length 15 mm, and a diameter of 8 mm. Then, it is heated above 45 °C, stretched and cooled down to the room temperature to fix a temporary shape with a length about 25 mm and a diameter of about 5 mm. This stretching is similar to the first cycle of the thermo-mechanical cycling described earlier with an increase of 75% of the foam's original length. The foam in this temporary shape is now able to easily penetrate a glass tube of 6 mm in diameter. When heated above 45 °C, by recovering its permanent shape, the foam efficiently seals the glass tube and prevents an aqueous solution to flow through the tube. This PCL-CAN foam presents the advantage of an externally

© 2022 The Author(s). Published by the Royal Society of Chemistry

Open Access Article. Published on 22 February 2022. Downloaded on 9/6/2025 6:56:05 AM.
This article is licensed under a Creative Commons Attribution-NonCommercial 3.0 Unported Licence.

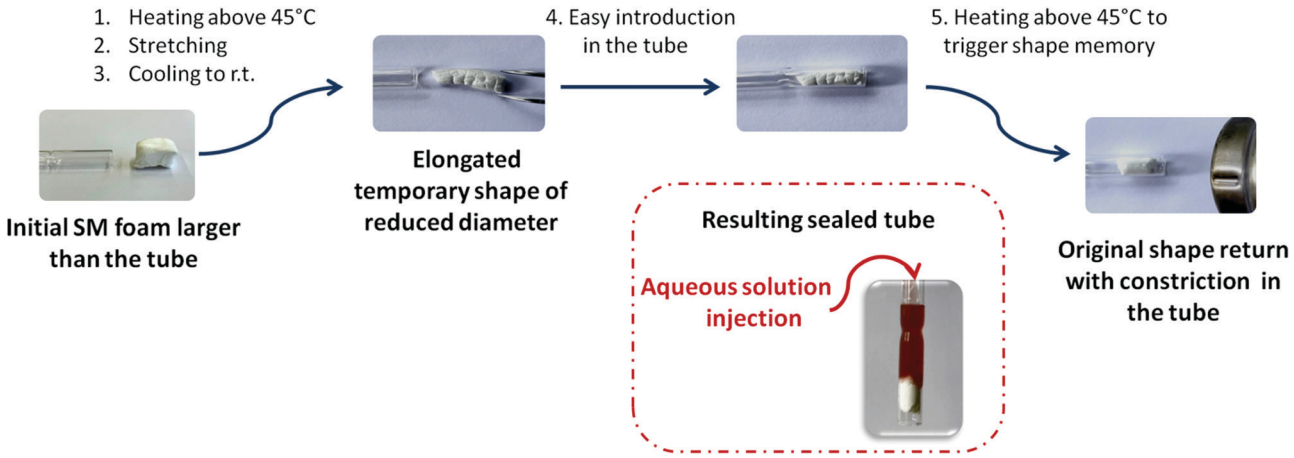

Fig. 8 Qualitative demonstration of a simulated vessel occlusion thanks to the shape-memory PCL-CAN foam. Video available in ESI.†

triggered expansion at temperatures closed to body temperature. Furthermore, thanks to the high volume expansion, the energy required to trigger that shape memory behavior is significantly lower as compared to less expanded devices.

Conclusions

In this work, a solvent-free $scCO_2$ batch foaming process was developed allowing preparation of PCL-CAN foams. These foams exhibit a remarkable low density (0.02 g cm^{-3}) keeping good mechanical properties thanks to the closed-cells morphology. Their covalent crosslinking achieved by post-curing the foam at 40 °C for a few days imparts these foams with excellent shape memory properties (high fixity and recovery ratios). The high temperature reversibility of the crosslinking of these PCL-CANs that include furane-maleimide Diels–Alder adducts in their structure makes them fully reprocessable. Advantage was taken from the thermal control of the furane-maleimide Diels–Alder addition to regulate the degree of branching and crosslinking of the starting end-functional PCL reactive mixture. The success of this foaming process relies on this precise control of crosslinking degree of the material at each step. These PCL shape memory foams are quite attractive for biomedical applications such as self-deploying implants for vessels occlusion, which was illustrated through dynamic mechanical analysis and mechanical occlusion of a large simulated vessel.

Conflicts of interest

There are no conflicts of interest to declare.

Acknowledgements

The research was founded through the ''Actions de recherche concertées 2017 – Synthesis, Characterization, and MultiScale Model of Smart composite Materials (S3CM3) 17/21-07'' financed by the ''Direction générale de l'Enseignement non obligatoire de la Recherche scientifique, Direction de la Recherche scientifique, Communauté française de Belgique, et octroyées par l'Académie Universitaire Wallonie-Europe''.

References

1 A. Mohebbi, F. Mighri, A. Ajji and D. Rodrigue, *Cell. Polym.*, 2015, **34**, 299–337.
2 D. Yin, J. Mi, H. Zhou, X. Wang and H. Tian, *Carbohydr. Polym.*, 2020, **247**, 116708.
3 Y. Qiao, Q. Li, A. Jalali, J. Yang, X. Wang, N. Zhao, Y. Jiang, S. Wang, J. Hou and J. Jiang, *Composites, Part B*, 2021, **208**, 108594.
4 C. X. Chen, H. H. Peng, Y. X. Guan and S. J. Yao, *J. Supercrit. Fluids*, 2019, **143**, 72–81.
5 G. Wang, J. Zhao, G. Wang, H. Zhao, J. Lin, G. Zhao and C. B. Park, *Chem. Eng. J.*, 2020, **390**, 124520.
6 J. Wang, J. Chai, G. Wang, J. Zhao, D. Zhang, B. Li, H. Zhao and G. Zhao, *Int. J. Biol. Macromol.*, 2019, **138**, 144–155.
7 R. Kuska, S. Milovanovic, S. Frerich and J. Ivanovic, *J. Supercrit. Fluids*, 2019, **144**, 71–80.
8 D. Valor, A. Montes, M. Monteiro, I. García-Casas, C. Pereyra and E. M. de la Ossa, *Polymer*, 2021, **13**, 1645.
9 D. G. Pyun, H. S. Yoon, H. Y. Chung, H. J. Choi, T. Thambi, B. S. Kim and D. S. Lee, *J. Mater. Chem. B*, 2015, **3**, 7752–7763.
10 Q. Gan, J. Zhu, Y. Yuan, H. Liu, Y. Zhu and C. Liu, *J. Mater. Chem. B*, 2015, **3**, 2281–2285.
11 F. V. Ferreira, C. G. Otoni, K. J. De France, H. S. Barud, L. M. F. Lona, E. D. Cranston and O. J. Rojas, *Mater. Today*, 2020, **37**, 126–141.
12 L. M. Marques, M. M. Alves, S. Eugénio, S. B. Salazar, N. Pedro, L. Grenho, N. P. Mira, M. H. Fernandes and M. F. Montemor, *J. Mater. Chem. B*, 2018, **6**, 2821–2830.
13 S. K. Han, M. Song, K. Choi and S. W. Choi, *Macromol. Mater. Eng.*, 2021, **306**, 1–10.
14 J. Hu, H. Albadawi, B. W. Chong, A. R. Deipolyi, R. A. Sheth, A. Khademhosseini and R. Oklu, *Adv. Mater.*, 2019, **31**, 1901071.

© 2022 The Author(s). Published by the Royal Society of Chemistry

Open Access Article. Published on 22 February 2022. Downloaded on 9/6/2025 6:56:05 AM.
This article is licensed under a Creative Commons Attribution-NonCommercial 3.0 Unported Licence.

15 P. Singhal, W. Small, E. Cosgriff-Hernandez, D. J. Maitland and T. S. Wilson, *Acta Biomater.*, 2014, **10**, 67–76.
16 E. Khodaverdi, M. Reza Abbaspour, F. Oroojalian, N. Omidkhah, S. Hossein-nezahd, H. Kamali and F. Hadizadeh, *J. Drug Delivery Sci. Technol.*, 2021, **66**, 102547.
17 J. Li, H. Wang, H. Zhou, J. Jiang, X. Wang and Q. Li, *ACS Omega*, 2021, **6**, 22672–22680.
18 J. A. Sarver and E. Kiran, *J. Supercrit. Fluids*, 2021, **173**, 105166.
19 T. Hatami, J. C. F. Johner, K. C. de Castro, L. H. I. Mei, M. G. A. Vieira and M. Angela, *Ind. Eng. Chem. Res.*, 2020, **59**, 20033–20044.
20 V. Santos-Rosales, M. Gallo, P. Jaeger, C. Alvarez-Lorenzo, J. L. Gómez-Amoza and C. A. García-González, *J. Supercrit. Fluids*, 2020, **166**, 105012.
21 A. Salerno, A. B. Leonardi, P. Pedram, E. Di Maio, M. A. Fanovich and P. A. Netti, *Mater. Sci. Eng. C*, 2020, **109**, 110518.
22 L. Baldino and S. Cardea, *Chem. Eng. Trans.*, 2020, **79**, 241–246.
23 M. Nofar, B. Batı, E. B. Küçük and A. Jalali, *J. Supercrit. Fluids*, 2020, **160**, 104816.
24 A. M. López-Periago and C. Domingo, *J. Supercrit. Fluids*, 2018, **134**, 204–213.
25 E. Di Maio and E. Kiran, *J. Supercrit. Fluids*, 2018, **134**, 157–166.
26 M. Chauvet, M. Sauceau and J. Fages, *J. Supercrit. Fluids*, 2017, **120**, 408–420.
27 A. Salerno, A. B. Leonardi, P. Pedram, E. Di Maio, M. A. Fanovich and P. A. Netti, *Mater. Sci. Eng. C*, 2020, **109**, 110518.
28 A. Salerno and C. Domingo, *J. Supercrit. Fluids*, 2019, **143**, 146–156.
29 C.-X. Chen, H.-H. Peng, Y.-X. Guan and S.-J. Yao, *J. Supercrit. Fluids*, 2019, **143**, 72–81.
30 R. Boia, P. A. N. Dias, J. M. Martins, C. Galindo-romero, I. D. Aires, M. Vidal-sanz, M. Agudo-barriuso, H. C. De Sousa, A. Francisco, M. E. M. Braga and A. Raquel, *J. Controlled Release*, 2019, **316**, 331–348.
31 K. Zhang, Y. Wang, J. Jiang, X. Wang, J. Hou, S. Sun and Q. Li, *J. Mater. Sci.*, 2019, **54**, 5112–5126.
32 A. Salerno, E. Di Maio, S. Iannace and P. A. Netti, *J. Supercrit. Fluids*, 2011, **58**, 158–167.
33 I. Tsivintzelis, E. Pavlidou and C. Panayiotou, *J. Supercrit. Fluids*, 2007, **42**, 265–272.
34 J. Thomassin, C. Pagnoulle, L. Bednarz, I. Huynen, R. Jerome and C. Detrembleur, *J. Mater. Chem.*, 2008, **18**, 792–796.
35 D. Pahovnik, *Macromolecules*, 2019, **52**, 9291–9298.
36 F. Zhang, T. Zhou, Y. Liu and J. Leng, *Nat. Publ. Gr.*, 2015, 1–12.
37 F. Quadrini, D. Bellisario, L. Santo, C. Del, A. Bianco, F. Quadrini, D. Bellisario, L. Santo and C. Del Gaudio, *Polym. – Plast. Technol. Eng.*, 2013, **52**, 599–602.
38 A. Salerno, E. Di Maio, S. Iannace and P. A. Netti, *J. Porous Mater.*, 2012, **19**, 181–188.
39 L. Lu, J. Cao and G. Li, *J. Appl. Polym. Sci.*, 2017, **45225**, 29–34.
40 G. M. Scheutz, J. J. Lessard, M. B. Sims and B. S. Sumerlin, *J. Am. Chem. Soc.*, 2019, **141**, 16181–16196.
41 C. J. Kloxin and C. N. Bowman, *Chem. Soc. Rev.*, 2013, **42**, 7161–7173.
42 M. K. McBride, B. T. Worrell, T. Brown, L. M. Cox, N. Sowan, C. Wang, M. Podgorski, A. M. Martinez and C. N. Bowman, *Annu. Rev. Chem. Biomol. Eng.*, 2019, **10**, 175–198.
43 G. Zhang, Q. Zhao, L. Yang, W. Zou, X. Xi and T. Xie, *ACS Macro Lett.*, 2016, **5**, 805–808.
44 T. Defize, R. Riva, C. Jérôme and M. Alexandre, *Macromol. Chem. Phys.*, 2012, **213**, 187–197.
45 T. Defize, R. Riva, J. M. Raquez, P. Dubois, C. Jérôme and M. Alexandre, *Macromol. Rapid Commun.*, 2011, **32**, 1264–1269.
46 T. Defize, J. M. Thomassin, M. Alexandre, B. Gilbert, R. Riva and C. Jérôme, *Polymer*, 2016, **84**, 234–242.
47 T. Dow, C. Company and D. B. Solutions, *J. Appl. Polym. Sci.*, 2014, **131**, 41293.
48 C. Marrazzo, E. Di Maio and S. Iannace, *Polym. Eng. Sci.*, 2008, **48**, 336–344.
49 K. Taki, D. Kitano and M. Ohshima, *Ind. Eng. Chem. Res.*, 2011, **50**(6), 3247–3252.
50 I. Tsivintzelis, A. G. Angelopoulou and C. Panayiotou, *Polymer*, 2007, **48**, 5928–5939.
51 L. J. White, V. Hutter, H. Tai, S. M. Howdle and K. M. Shakesheff, *Acta Biomater.*, 2012, **8**, 61–71.
52 C. X. Chen, Q. Q. Liu, X. Xin, Y. X. Guan and S. J. Yao, *J. Supercrit. Fluids*, 2016, **117**, 279–288.
53 T. Chung, A. Romo-uribe and P. T. Mather, *Eur. Polym. J.*, 2008, **41**, 184–192.
54 G. Floudas, L. Hilliou, D. Lellinger and I. Alig, *Macromolecules*, 2000, **33**, 6466–6472.
55 J. Diani and K. Gall, *Society*, 2006, **46**, 486–492.
56 S. M. Hasan, G. K. Fletcher, M. B. B. Monroe, M. A. Wierzbicki, L. D. Nash and D. J. Maitland, *Polymers*, 2020, **12**, 1–16.

© 2022 The Author(s). Published by the Royal Society of Chemistry